Computer modelling of a penetrator thermal sensor

Journal Item

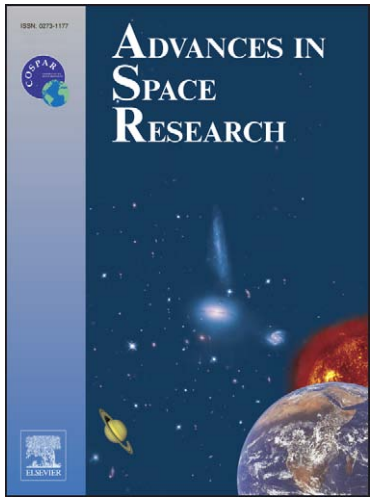

Computer modelling of a pentrator thermal sensor

M.D. Paton, G. Kargl, A.J. Ball, S.F. Green, A. Hagermann, N.I. Kömle, M. Thiel, J.C. Zarnecki

PII: S0273-1177(10)00178-X
DOI: 10.1016/j.asr.2010.03.007
Reference: JASR 10117

To appear in: *Advances in Space Research*

Received Date: 8 August 2008
Revised Date: 14 January 2010
Accepted Date: 4 March 2010

Please cite this article as: Paton, M.D., Kargl, G., Ball, A.J., Green, S.F., Hagermann, A., Kömle, N.I., Thiel, M., Zarnecki, J.C., Computer modelling of a pentrator thermal sensor, *Advances in Space Research* (2010), doi: 10.1016/j.asr.2010.03.007

Computer modelling of a pentrator thermal sensor

M. D. Paton[a], G. Kargl[b] , A. J. Ball[a], S. F. Green[a], A. Hagermann[a], N. I. Kömle[b], M. Thiel[c] and J. C. Zarnecki[a]
[a]*Planetary and Space Sciences Research Institute, The Open University, Walton Hall, Milton Keynes, MK7 6AA, UK*
[b]*Space Research Institute, Austrian Academy of Sciences, Schmiedlstrabe 6, A-8042, Graz, Austria*
[c]*Max-Planck-Institut für Extraterrestrische Physik, Giebenbachstrabe, 85748 Garching, Munich, Germany*

Corresponding author email: mark.paton@helsinki.fi or markipaton@hotmail.co.uk

Abstract

The Philae lander is part of the Rosetta mission to investigate comet 67P/Churyumov-Gerasimenko. It will use a harpoon like device to anchor itself onto the surface. The anchor will perhaps reach depths of 1-2 m. In the anchor is a temperature sensor that will measure the boundary temperature as part of the MUPUS experiment. As the anchor attains thermal equilibrium with the comet ice it may be possible to extract the thermal properties of the surrounding ice, such as the thermal diffusivity, by using the temperature sensor data. The anchor is not an optimal shape for a thermal probe and application of analytical solutions to the heat equation is inappropriate. We prepare a numerical model to fit temperature sensor data and extract the thermal diffusivity. Penetrator probes mechanically compact the material immediately surrounding them as they enter the target. If the thermal properties, composition and dimensions of the penetrator are known, then the thermal properties of this pristine material may be recovered although this will be a challenging measurement. We report on investigations, using a numerical thermal model, to simulate a variety of scenarios that the anchor may encounter and how they will affect the measurement.

Keywords: penetrator, comet, Rosetta, modelling, thermal, sensor

1. Introduction

Rosetta is an ESA mission to study comet 67P/Churyumov-Gerasimenko (Glassmeier et al., 2007). It includes a lander, Philae that is expected to land on the comet at 3 AU from the Sun in November 2014. Rosetta will accompany the comet to perihelion at 1.3 AU studying the nucleus properties, the physiochemical evolution of the coma and the plasma environment. Philae will provide a ground truth to the measurements made in orbit. It will do this by sampling material from the nucleus that may be pristine. Such material holds the key to understanding the formation of comets and is also thought to be preserved from the formation of the Solar System. Philae includes a thermal experiment called MUPUS (Spohn et al., 2006) that will contribute to assessing the energy balance of the comet nucleus and measure the physical properties of its material that will include the thermal diffusivity and thermal conductivity. These measurements are strong functions of the comet ice structure and

will determine to what degree the structure has been thermally altered and constrain whether other instruments on Philae are sampling pristine comet ice.

Upon touchdown Philae will fire a harpoon-like device (see figure 1) at about 60 m s^{-1} into the comet ice to anchor itself onto the surface. Contained within the anchoring device are two MUPUS sensors, an accelerometer and a PT100 temperature sensor. The primary role of the temperature sensor is to measure the equilibrium temperature 1-2 m below the surface and thus provide a boundary condition for thermal investigations closer to the surface.

Figure 1

Figure 2

Penetrators, like the anchor and MUPUS thermal probe, are well suited to delivering thermal instruments, remotely, into planetary surfaces that have uncertain mechanical properties. Similar devices have been proposed or have been included on other space missions, although none have been successfully deployed, employing a variety of deployment techniques such as ballistic delivery (e.g. Urquhart et al., 2000, Tanaka et al., 2001) or hammering (Spohn et al., 2001, Spohn et al., 2007).

On Earth a popular method for measuring thermal properties of materials, such as soils, liquids and gases, is the line-heat source. An infinitely long cylindrical heat source can be modelled using an analytical solution to the heat equation. This geometry can be approximated using a long cylindrical probe, typically in the order of 1 mm in width and perhaps 200 mm in length, fitted with a heating element that is coupled with a temperature sensor. The temperature profile with time can then be used to derive the thermal conductivity of the material probed. The probe has to be driven slowly into a sample avoiding large stresses on the structure and so is unsuitable for a planetary surface that is poorly characterised or if inserted at high speed. See Seiferlin et al. (1996) for a short review and application of the technique to the measurement of the conductivity of ice and mineral powders under space conditions.

The hot wire method is similar to the probe method except the heating element doubles up as a temperature sensor. The wire is thin so care has to be taken over its use and it is best suited to measuring thermal conductivity in gases and liquids (e.g. Birchley et al., 1992). Another method similar to the hot-wire method, but based on a different geometry, is the spherical heat source. Due to its small size it is best suited to liquids and consolidated materials (van Gelder, 1998). All these methods use an active heat source. The guarded torus (Seiferlin, 2006) has been investigated, using a numerical modelling technique, as a transient method to enable effective in situ thermal measurements.

Thermal properties, such as thermal conductivity and thermal inertia, can also be measured by monitoring the temperature of a probe-type device as it attains thermal equilibrium with its surroundings (Bullard, 1954).

The anchor was primarily designed to penetrate and remain embedded in the surface so is not an optimised shape for thermal property measurements. To model a thermal probe with a complex shape a numerical model is required. Successful implementation of this technique crucially depends on knowing the thermal properties of the anchor, understanding the heat transfer processes on the comet and an awareness of possible mechanical disturbances by the anchor.

2. Modelling using numerical techniques

The control (or finite) volume method is used for solving partial differential equations applied to complicated fluid and thermal flow problems. Here a thermal model is constructed by dividing the anchor and surrounding comet ice into volume elements each assigned with their own set of thermal properties. A discrete version of the heat equation is then used to solve for each control volume. Choosing an appropriate coordinate geometry and number of dimensions for the element grid helps optimise computing efficiency by reducing the number of control volumes. The anchor can be mapped onto a grid that is axial symmetric. In the 2D cylindrical coordinates of radial distance (r) and depth (z) the heat equation is expressed as follows,

$$\rho c \frac{\partial T}{\partial t} = \frac{1}{r}\frac{\partial}{\partial r}\left(kr \frac{\partial T}{\partial r} \right) + \frac{\partial}{\partial z}\left(k \frac{\partial T}{\partial z} \right) + S \qquad (1)$$

where k is the conductivity, ρ is the density, c is the heat capacity, S is heat production and T is the temperature. The thermal quantities ρc and k can be varied to fit the model to the measurements. However as there are two unknowns only the ratio, diffusivity (eqn 2) is the only meaningful and useful thermal property that can be extracted from the model.

$$\alpha = \frac{k}{\rho c} \qquad (2)$$

A discrete version of the heat equation is used to compute the temperature in each volume element after each time step. The implicit scheme is used to compute the temperature (e.g. see Patankar, 1990). In the implicit scheme the temperature step across the time interval matches the exponential behaviour of temperature variations intrinsic in nature more closely than the explicit and Crank-Nicolson schemes. Also the implicit method will not produce physically meaningless results due to mathematical instabilities inherent in the other methods.

2.1 The Philae anchor model

To model the anchor the volume elements can in principle be decreased in size until they are comparable to the tiniest variations on the anchor's surfaces and internal components. This requires an enormous number of control volumes and is impractical in terms of the computing time or the time required generating the model of the anchor in the first place. Simplifying the structure of the model by removing all small components that are thermally insignificant, can help reduce the number of volume elements and reduce the computing time. Figure 3 shows a simplified model of the anchor that can easily be mapped onto such a control volume grid.

The anchor body consists of a cylinder and a conical tip. The barbs protruding from the anchor tip (see figure 1) have a large surface area to mass ratio and are efficient dissipaters of heat. Their small attachment area however restricts the transfer of heat from the anchor. A similar situation occurs when the flaps (see figure 2) are deployed. It is unclear how this will affect the heat transfer. The barbs and flaps can

be approximately modelled in two-dimensional axial symmetric geometry by attaching a disc with the same surface area and attachment cross-section to the anchor nose and body.

Figure 3

The efficiency of the heat transfer processes, conduction, convection and radiation, depends on the temperature difference between the materials under consideration. Removing inefficient processes from the computer model can speed up the calculations. It is not clear what contribution radiation will make to the heat transfer. A simple one-dimensional model, shown in figure 4, has been constructed to examine heat transfer mechanisms of conduction and radiation inside the anchor.

Figure 4

The thermal equation for radiation along path 1 in figure 4 is

$$q_r = \varepsilon A \sigma \left(T_s^4 - T_c^4 \right) \tag{3}$$

where T_s is the temperature of temperature sensor, T_c is the comet temperature (arbitrarily was set at 120 K in this work), ε is emissivity (set to 1 for a worst case scenario), A is the area of heat sensor in contact with accelerometer (5.85×10^{-6} m^{-2}) and σ is Stefan's constant. The thermal equation for conduction along path 2 (see figure 4) is,

$$q_k = kA \frac{T_s - T_c}{x_k} \tag{4}$$

where k is thermal conductivity of the tip (400 W m^{-1} K^{-1} for CuBe2), x_k is the distance between the temperature sensor and the comet ice (~4 mm). The energy lost by radiation was found to be only 0.01% of that lost by conduction. Even when the comet ice was set at a temperature close to the anchor the heat loss by radiation was found to be only about 0.1% of that lost by conduction into the anchor body.

The thermal conductivity of a material is dependant on its temperature. Data of the thermal conductivity and heat capacity dependence on temperature for various materials are available from The National Institute of Standards and Technology (NIST). They use polynomial and logarithmic polynomial equations and fit them to data acquired from past publications and present the results for anyone to use (Marquardt et al., 2000). These equations were used in the thermal model to calculate the thermal conductivity and heat capacity of the anchor assuming the complete anchor was made of CuBe2.

The temperature sensor will lose or gain heat through the electrical wires connected to the spacecraft. The amount of heat transferred will depend on the thickness of the wires and the temperature gradient along the wires. All six wires in the anchor cable are AWG 36 with a diameter of 0.127 mm (Stöcker and Thiel, 1997). The amount of heat lost through the two wires connected to the temperature sensor can then be estimated by assuming some temperature gradient along the wires. The surface area for a long thin cylindrical structure, like wires, is many magnitudes of

order larger than its cross-sectional area and so will attain thermal equilibrium with its surroundings very quickly. A plausible situation would then be if the wires cool to the same temperature as the surrounding comet ice outside the anchor and remains at the anchor temperature at the electronics connection with the sensor. The heat flow out of the temperature sensor can then be approximately modelled using the following equation.

$$q_k = k_w A_w \frac{T_s - T_w}{x_w} \tag{5}$$

where k_w is the conductivity of the wire (copper), A_w is the cross-sectional area of the wire, T_s is the temperature at the wire at distance x_w from the sensor which is the length of the anchor body, 90 mm. The thermal conductivity of copper between 120 K and 160 K is relatively constant at about 400 W m^{-1} K^{-1}. Using these values the heat loss will be approximately 3% of that lost through conduction from the sensor into the anchor body.

2.2 The comet ice model

Observations of cometary surfaces by spacecraft have revealed very dark surfaces and nuclei of low bulk density. Excavation of Tempel 1 by a projectile carried by the Deep Impact spacecraft suggests a nucleus with volatiles hidden below a thin mantle of fine powdery material (A'Hearn et al., 2005). The surface of 67P/Churyumov-Gerasimenko is characteristically similar to 9P/ Tempel 1 in terms of its phase function and it is anticipated to have a similar thermal inertia (Lamy et al., 2006). The internal structure of comet nuclei is poorly known but the bulk density of comets is very low indicating high macro porosity, high micro porosity or a combination of both. The Philae anchor may help answer structural questions using its accelerometer (Kömle et al., 2001). It is reasonable to assume that 67P/Churyumov-Gerasimenko surface will be similar to current models of comets with a layer of volatile depleted hydrocarbon dominated surface with icy material below. As Philae will land at about 3 AU from the Sun, the surface will be relatively inert (Glassmeier et al., 2007).

Comet nucleus material can be modelled as a highly porous agglomeration of grains made of volatile ices and dust, with a size distribution that probably spans many orders of magnitude. When a comet approaches the sun sintering processes will cause movement of volatiles from concave to convex surfaces so strengthening the necks between particles and the fusing of the ice grains together (e.g. Ratke et al., 1992). A measure of the cohesiveness is the Hertz factor. The variable is defined as the ratio between the grain-to-grain contact area and the cross-section of the grain. A full treatment of the conductivity including parameters such as porosity, the shape of the pores, the grain size, the size of the contact areas, and local density should ideally be established. These parameters can be referred to as the texture. See Kargl (1998) for a full discussion.

Figure 5 shows two possible material structures that could be found in a comet. The granular material is a collection of loose grains that were formed by impacts or are pristine grains from comet formation. The cellular material represents thermally altered ice grains where sintering has deposited material around the contact points.

Figure 5

When disturbed by the penetrating projectile the thermal properties of the two materials may change in different ways, shown in figure 5. For a loose granular material the grains will become more tightly packed with more contacts, increasing the Hertz factor and the ability to conduct heat. The porosity is decreased but this has no additional influence on the conduction as there is no gas or liquid to conduct heat across the pores. However this effect will be difficult to see as we are measuring the diffusivity where the bulk density is in the denominator (see equation 2). Compaction will increase the bulk density which could effectively cancel out the effect of the increase in conduction.

The bonds in a cellular material will have to be broken to allow the projectile to pass which will decrease the contact area overall between grains even though there may be extra contact points. The Hertz factor and the thermal conductivity will then be reduced. As the bulk density increases, due to compaction, this will have the effect of significantly reducing the diffusivity.

In our thermal model a locally homogeneous medium is considered because we are unlikely to recover any information about inhomogeneities due to the small size of the anchor. An effective conductivity can be formulated modelling the comet material as a silicate grain with an icy mantle (e.g. Sirono and Yamamoto, 1997). As the microstructural distribution of material is unknown we assumed that the comet material is pure ice. The relationship for the conductivity for compact ice can be expressed as dependant on the temperature as determined empirically by Klinger (1981). Many attempts have been made to model the thermal conductivity of porous ice using textural information (Seiferlin, 1990). Porosity only becomes an important factor at temperatures above 200 K due to heat transfer across the pore space by convection and radiation (Seiferlin et al., 1996). In our work we can keep things simple due to the low temperatures used and model the texture only with the dimensionless Hertz factor, h.

$$k = \frac{567h}{T} \quad \text{W m}^{-1}\,\text{K}^{-1} \tag{6}$$

where T is the temperature of the ice.

The heat capacity for porous ice remains the same as for solid ice and is expressed as the temperature dependent equation,

$$c = 90 + 7.49T \quad \text{J kg}^{-1}\,\text{K}^{-1} \tag{7}$$

The density of comet ice will be dependent on its mineralogical content, its bulk porosity and internal grain porosity. The bulk porosity of comets is poorly constrained and could ideally be measured in-situ (e.g. Ball et al, 2001). The density of a porous material can be expressed as follows,

$$\rho = \rho_S(1-\phi) \tag{8}$$

where ρ_S is the density of the material with zero porosity and ϕ is the porosity of the material. The bulk density of comet nucleus has been measured for several comets with results varying from anywhere between 100 to 900 kg m^{-3} with a convergence to lower values, typically 500 kg m^{-3}. An estimated density for 67P/Churyumov-

Gerasimenko is 370 kg m^{-1} (Lamy et al., 2007). It is however unrealistic to assume that the thermally altered surface and immediate sub-surface, down to a few metres, will have a bulk density the same as the nucleus. Radio observations of comets suggest the surface density is in the 500 to 1000 kg m^{-3} range (Harmon and Nolan, 2005). For this work we have assumed a solid density of water ice, 920 kg m^{-3}, and a porosity of 0.5. This gives a value of 410 kg m^{-3} for the sub-surface density. Comet sub-surface material will probably be a mixture of mostly of water ice and silicate materials raising the bulk density somewhat but strictly speaking we do not know what material the anchor will be embedded in and water ice is a well characterised material in the literature.

At the surface the comet temperature may be as high as 163 K at 3 AU from the Sun (Blecka et al., 2003). Heat transfer by vapour transport was not included in the calculation because the temperatures considered (<200K) are low enough to be negligible (Seiferlin et al., 1996). Heat transfer by radiation was shown to be very small in section 2.4 inside the anchor and has been noted by Thomas and Spohn (2002) as negligible for comet ice at the low temperatures we consider here.

The equations for thermal conductivity, heat capacity and density the temperature dependent diffusivity can be combined as,

$$\alpha = \frac{567h}{\rho_S \left(1-\phi\right)\left(90T + 7.49T^2\right)} \quad \mathrm{m^2\ s^{-1}} \tag{9}$$

The solid density of the ice is known (if it is ice) or may be inferred from other measurements on Rosetta. Unfortunately the densitometer that was to be included on the MUPUS thermal probe was cancelled due to funding problems (Spohn et al., 2007). The temperature of the ice can be measured directly once the anchor has reached equilibrium with its surroundings. The ratio of Hertz factor over one minus porosity is the greatest unknown. The Hertz factor may possibly range over an order of magnitude from 0.01 to 0.3 for sintered grains (Kossacki et al., 1999). For granular material the porosity may range only between 0.3 and 0.5 (Paton, 2005). From equation 9 it can be seen that the diffusivity will be particularly sensitive to the Hertz factor.

The anchor will disturb the ice in several ways during penetration. The anchor body will expand a cavity in the ice forming a layer of compacted material surrounding the projectile. The barbs will churn up material around the anchor. Shovelling of material by the flaps will occur as the tether is tightened, compacting and disturbing the material through shearing. The contacts between grains will be broken during penetration and so possibly lower the diffusivity even though the grains around the anchor are compacted.

Figure 6

The thickness of compacted material surrounding the cylindrical body of the anchor can be estimated by tracking the undisturbed material from the formation of a cylindrical cavity (e.g. Johnson, 2001). The equation for the outer radius of the compacted material in terms of porosity is,

$$r_2 = r_1\sqrt{\frac{1-\phi_f}{\phi_0-\phi_f}} \quad (10)$$

where r_1 is the radius of the anchor, Φ_0 is the initial porosity and Φ_f is the final porosity.

The random packing of monodisperse spheres is well studied, with a packing density (amount of solid material in a given volume) of 0.64, equivalent to a porosity of 0.36 (Torquato et al., 2000). For naturally produced grains the porosity will be dependant on the size distribution, particle shape and surface texture. For a terrestrial material such as gravel the minimum porosity can vary between 0.33 and 0.36 (e.g. Paton, 2005). On the Moon the minimum porosity is much larger varying between 0.32 and 0.48 (Heiken et al., 1991). Particles on the Earth are rounded by weathering processes whereas on the Moon these processes are absent so the particles are more angular and can resist shearing forces by locking. When the anchor penetrates the comet surface it will break the intergranular bonds creating angular particles that are perhaps difficult to compact.

3. Computer modelling results

To determine the cooling time of the anchor and investigate the sensitivity of the results on the microstructural properties (intergranular contacts and porosity) the anchor was placed in undisturbed comet ice and allowed to cool. The simulation results in figure 7 show the temperature at the location of the anchor's PT100 sensor. The Hertz factor is an important indicator of the thermal alteration of the comet ice and may help asses how pristine the comet ice is around the Philae landing site. To investigate the sensitivity of the results on the microstructural properties (inter-granular contacts and porosity) the anchor was placed in undisturbed comet ice and allowed to cool.

The simulation results in figure 7 show the temperature at the location of the anchor's PT100 sensor. Temperatures when using a low Hertz factor are higher than those when using a high Hertz factor. This makes physical sense as a large Hertz factor models a large intergranular contact enabling a greater rate of heat to flow through the ice. The anchor cools more quickly in low porosity ice than in high porosity ice. This is to be expected because compact, low porosity, material will have more contacts between the grains providing more paths for the heat to flow away from the anchor. The difference between models with highly sintered grains (h=0.1) and poorly sintered grains (h=0.01) are quite well separated even with large variation in porosity. The thermal diffusivity for the cases where Φ_0=0.5 and h=0.01 and h=0.1 are 1.04 x 10^{-7} m^2 s^{-1} and 1.04 x 10^{-6} m^2 s^{-1} respectively.

Figure 7

When the anchor tip penetrates the ice it will push material to the side and compact it. To examine the effect of the compaction zone on the cooling rate first a simulation was run where the anchor is placed in the ice and there is no compaction. Then simulations were run with a compaction zone around the anchor simulated using control volumes with their own unique set of thermal properties. The radial extent of the compaction zone was calculated using equation 9. The compacted comet ice was

assumed to be granular in nature cemented together by sintering and compacted from a porosity of 0.5 to either 0.4 or 0.3. For a Hertz factor, h=0.01, this corresponds to a 16% and 28% difference in the thermal diffusivity with the non-compacted ice. Laboratory experiments using a low speed penetrator at 1 m s^{-1} into loose granular materials (chalk powder and metal powder) increase the thermal diffusivity by only around 5% (Paton, 2005). Therefore it might be quite difficult for the anchor to compact material by any significant amount.

The Philae anchor will most likely penetrate comet ice grains that are fused together breaking the bonds between them decreasing the Hertz factor by an order of magnitude. However it is not clear what effect the breaking of bonds between the grains will have on the intergranular contacts as the porosity will be decreased. To help asses the effect simulation were run were the Hertz factor, in the compaction zone, was varied upwards and downwards, the results shown in figure 8.

Figure 8

A compaction zone drastically perturbs the cooling of the anchor (compared to the no compaction case) when the Hertz factor is varied up and down by a factor of 2 as seen in figure 8. In comparison the porosity has little effect. A compaction zone with lower porosity (long-dash line compared to short-dash line in figure 8) will have a smaller relative effect due to its smaller size. The important properties of the surrounding comet ice are then the thermal diffusivity of the compaction zone and the size of the compaction zone.

It may be possible to extract the thermal properties of the compaction zone from the first few seconds of cooling before heat from the anchor reaches the non-compacted material. This could be done by fitting output from a model with an anchor in a non-compacted ice (i.e. like the no compaction case in figure 8) to the model whose compacted zone has the same thermal properties. It may become a particularly useful exercise if measurement errors or data loss reduces the quality of the data over long periods of time that will be required to fit a model which includes a compaction zone.

To examine this possibility a series of simulations were run with anchors in compaction zones of different sizes that were then compared to anchors in ice with the same thermal properties as the compacted zone but with an infinite radius (i.e. nominal case). In the case of the finite compaction zone the undisturbed ice thermal properties were kept constant throughout the simulation campaign. The differences in the anchor cooling rates are shown in figure 9. For the first few seconds the cooling in both the finite and infinite compaction zone are the same. It may then be possible to determine the thermal diffusivity of the compaction zone in the first few seconds of cooling before the heat is transferred into the non-compacted comet ice.

Figure 9

To secure the lander to the surface the anchor tether will be tightened causing the shovel flaps to open up, possibly fully in weak material, compacting material above the flaps. The anchor has barbs on its nose that will resist pulling when the tether is tightened. If the barbs cannot provide the necessary resistance the flaps will open up. Whether they open or not then depend on how well the barbs stick in the ice, which

cannot be known. It is therefore important to know how the deployed flaps affect the cooling of the anchor.

Figure 10 shows results comparing models of anchors with stowed and deployed flaps. For comet ice with poorly sintered grains (h=0.01) the anchor with flaps deployed cools the fastest but the temperature gradually approaches the anchor with flaps stowed. For comet ice sintered grains (h=0.1) the anchor with flaps deployed cools fastest initially and then slows being overtaken by the anchor with flaps stowed. The anchor flaps provides a path for heat to escape quickly and spread out into the ice. Over long time periods the two anchor models converge to similar temperature and rates of cooling.

Figure 10

4. Conclusions

A numerical model of the Philae anchor has been developed as a means to determine thermal diffusivity of the comet ice by fitting a model to temperature sensor data. Various scenarios, including a compaction zone around the anchor and an anchor with deployed flaps, were simulated to asses the thermal behaviour of the anchor in comet ice.

It was found that the thermal response of the anchor is weakly sensitive to the porosity of the comet ice while strongly affected by the Hertz factor. The Hertz factor of the comet ice may be significantly different to the Hertz factor of compacted ice around the anchor. Therefore a compaction zone needs to be accounted for when deriving the thermal diffusivity of the undisturbed comet ice. As the Hertz factor will be the dominant parameter in fitting model to the data it is in principle possible to comment on the thermal alteration state of the comet ice around the anchor in a qualitative way, perhaps together with some constraint on the Hertz factor.

It is possible that the thermal diffusivity of the compaction zone could be determined in the first few seconds after the anchor enters the comet ice aiding the interpretation the temperature sensor data. An anchor with deployed flaps increases the cooling rate and ideally needs to be accounted for when modelling the anchor.

A high rate of sampling (perhaps once a second) is required in the first 10 s to determine the properties of the compaction zone. A long period of sampling is required (hours) to determine the properties of the undisturbed material.

References

A'Hearn, M. F., Belton, M. J. S., Delamere, W. A., et al., Deep Impact: Excavating Comet, 2005, Tempel 1, Science, 310, 258-264

Ball, A. J., Gadomski, S., Banaszkiewicz, M., et al., An instrument for in situ comet nucleus surface density profile measurement by gamma ray attenuation, Planetary and Space Science, 49, 961-976, 2001

Blecka, M. I., Capria, M. T., Coradini, A., et al., Numerical simulations of the radiance from Comet 46P/Wirtanen in the various configurations of the measurements during "Rosetta" mission, Advances in Space Research, 31, 2501-2510, 2003

Bibring, J. P-., Rosenbauer, H., Boehnhardt, H., et al., The Rosetta lander ("Philae")

investigations, Space Science Reviews, 128, 205-220, 2007
Biele, J. and Ulamec, S., Capabilities of Philae, the Rosetta lander, Space Science Reviews, 138, 275-289, 2008
Bullard, E. C., The flow of heat through the floor of the Atlantic Ocean, Proc. R. Soc. London, Series A, 222, 408-425, 1954
Capria, M. T., Coradini, A., de Sanctis, M. C. Modelling of cometary nuclei: Planetary missions preparation, Advances in Space Research, 31, 2543-2553, 2003
Glassmeier, K-H., Boehnhardt, H., Koschny, D., et al., The Rosetta mission: Flying towards the origin of the Solar System, Space Science Reviews, 128, 1-21. 2007
Harmon, J. K. and Nolan, M. C., Radar observations of Comet 2P/Encke during the 2003 apparition, Icarus, 176, 175-183
Heiken, G. H., Vaniman, D. T., French, B. M., Lunar Sourcebook: A user's guide to the moon, Cambridge University Press, Cambridge, 1990
Johnson, J. B., 2001 A physically based penetration equation for compressible materials, In: Komle, N.I., Kargl, G., Ball, A.J., Lorenz, R.D. (Eds), Penetrometry in the Solar System, Austrian Academy of Sciences Press, Vienna
Kadano, T., Sugita, S., Sako, S., et al., The thickness and formation age of the surface layer on comet 9P/Tempel 1, The Astrophysical Journal, 661, 82-92, 2007
Kargl, G. Physical processes on the surface of a cometary nucleus: experimental investigation of the influence of organic constituents on the thermal properties, Doctoral Thesis, Space Research Institute, Austrian Academy of Sciences, 1998
Kömle, N. I., Kargl, G., Ball, A. J., Determination of physical properties of planetary sub-surface layers by artificial impacts and penetrometry, Advances in Space Research, 20, 1539-1549, 2001
Klinger, J. Some consequences of a phase transition of water ice on the heat balance of comet nuclei, Icarus, 47, 320-324, 1981
Kossacki, K. J., Szutowicz, S., Leliwa-Kopystynski, J., Comet 46P/Wirtanen: evolution of subsurface layers, Icarus, 142, 202-218, 1999
Lamy, P. L., Toth, I., Davidsson, B. J. R. et al., A portrait of the nucleus of comet 67P/Churyumov-Gerasimenko, Space Science Reviews, 128, 23-66, 2007
Marquardt, E. D., Le, J. P, Radebaugh, R., Cryogenic Material Properties Database, 11th International Cryocooler Conference, June 20-22, 2000
Patankar, S. V. Numerical heat transfer and fluid flow, McGraw-Hill Book Company, New York, 1990
Paton, M. D., 2005, Penetrometry of NEOs and other Solar System bodies, PhD thesis, the Open University, UK
Ratke, L., Kochan, H., Thomas, H., Laboratory studies of cometary crust formation: The importance of sintering, Asteroids, Comets, Meteors, Houston, 1992
Seiferlin, K., The thermal conductivity of porous ice with application to KOSI sample material: a review, Theoretical Modelling of Comet Simulation Experiments , N. I. Komle, S.J. Bauer, and T. Spohn (Ed), Proceedings of the KOSI modeller's workshop, 1990
Seiferlin, K., Komle, N. I., Kargl, G., et al., Line heat-source measurements of the thermal conductivity of porous H_2O ice, CO_2 ice and mineral powders under space conditions, Planet, Space Sci., 44, 691-704, 1996
Seiferlin, K., The guarded torus: Numerical model of a novel transient method for thermal conductivity measurements. Measurement, Science and Technology, 17, 3083-3093, 2006

Sirono, S. and Yamamto, T., 1997, Thermal conductivity of granular materials relevant to the thermal evolution of commentary nuclei, Planetary and Space Science, 45, 827-834

Spohn, T., Karsten, S., Hagermann, A., et al., MUPUS – A thermal and mechanical properties probe for the Rosetta lander Philae, Space Science Reviews, 128, 339-362, 2007

Spohn, T., Ball, A. J., Seiferlin, K., et al., A heat flow and physical properties package for the surface of Mercury, Planetary and Space Science, 49, 1571-1577, 2001

Steiner, G., Two considerations concerning the free molecular flow of gases in porous ice, Astronomy and Astrophysics, 240, 533-536, 1990

Stöcker, J. and Thiel, M., 1997, ROSETTA lander subsystem specification Work Package 5350: ANCHORING SYSTEM, RO-LAS-SP-3101, Issue 3, MPE Garching

Tanaka, S.; Yoshida, S.; Hagermann, A., et al., In Situ Lunar Heat Flow Experiment Using the LUNAR-A Penetrator, 32nd Annual Lunar and Planetary Science Conference, March 12-16, 2001, Houston, Texas, abstract no.1495

Thomas, K. and Spohn, T., Theoretical aspects and interpretation of thermal measurements concerning the subsurface investigation of a cometary nucleus, Planetary and Space Science, 50, 929-937, 2002

Torquato, S., Truskett, T. M., Debenedett, P. G., Is random close packing of spheres well defined?, Physical Review Letters, 84, 2064-2067, 2000

Urquhart, M. L. and Smrekar, S. E. Estimation of soil thermal conductivity from a Mars microprobe-type penetrator, 31st Annual Lunar and Planetary Science Conference, March 13-17, 2000, Houston, Texas, abstract no. 1781

van Gelder, M. F., 1998, A thermistor based method for measurement of thermal conductivity and thermal diffusivity of moist food materials at high temperatures, PhD thesis, Virginia Polytechnic Institute and State University

Woodside, W., Calculation of the thermal conductivity of porous media, Canadian Journal of Physics, 36, 815-817, 1958

Figure 1 The Philae anchor in its housing (Photo: Markus Thiel). The tip of the anchor is exposed, covered with barbs. The barbs are to help the anchor remain embedded in the comet ice.

Figure 2 The Philae anchor with the flaps opened up and the tip disconnected from the shaft revealing the accelerometer with electrical wires (Photo: Markus Thiel). The temperature sensor is located in a borehole in the tip which is made of Copper-Beryllium (CuBe2). The flaps will open up if the comet ice is very soft.

Figure 3 Axial symmetric models of the anchor. On the left is a cross-section of the anchor, viewed from the side, with the flaps in a stowed position (A). The central diagram shows a cross-section of the anchor, viewed from the side, with the flaps deployed (B). On the right is a cross-section of the anchor, viewed from the top, with the flaps modelled as a disc with the same surface area and mass as the real anchor flaps. The anchor tip is modelled as a cone with a length of 60 mm and an opening angle of 15º. The base of the tip was 15 mm in diameter from which a cylindrical shaft, 90 mm in length, extended. The temperature sensor is located in a borehole in the tip (Stocker and Thiel, 1998). A cylindrical sub-section was removed from the inside leaving an opening in the top of the anchor 8 mm in diameter and 60 mm deep.

Figure 4 A simplified one-dimensional thermal model of the anchor. On the left is a cross-section of the anchor showing possible paths for heat transfer by radiation (Path 1) and conduction (Path 2). On the right is a detailed model with the components under consideration.

Figure 5 Two extreme forms of possible cometary material. Material 1 consists of ice grains while material 2 is cellular ice formed by sintering. The top diagrams show pristine material while the bottom layer shows material pushed to the side and compacted by the anchor. The grains are pushed together while the cellular material is broken into fragments. To compact material 1 the grains are moved closer together while to compact material 2 the bonds have to be broken into fragments. For material 1 the Hertz factor and porosity of compacted and non-compacted ice have relative values such that $h_2 > h_1$ while $\Phi_2 < \Phi_1$ and for material 2 $h_4 < h_3$ while $\Phi_4 < \Phi_3$.

Figure 6 Compacted zone around the anchor due to penetration. As the tip enters material is pushed to the side forming a compaction zone of disturbed material with an outer radius of r_2 and an inner radius of r_1.

Figure 7 Cooling simulation of the Philae anchor in non-compacted comet ice. The temperatures are from the location of the temperature sensor where the initial temperature of the anchor has been normalised to one and the initial temperature of the ice has been normalised to zero. The porosity of the comet ice, Φ_0, was varied from 0.3 to 0.7 approximately covering possible comet porosities. The Hertz factor used was 0.01 for grains with poor thermal connections and 0.1 with strong thermal connections.

Figure 8 Cooling of the anchor surrounded by a compaction zone. The coloured lines represent simulations with a compaction zone where r_2 is the outer radius of the compaction zone, Φ_c is the porosity of the compacted zone, h_c is the Hertz factor for the compacted zone, Φ_0 is the porosity of the non-compacted ice and h_0 is the Hertz factor for the non-compacted ice.

Figure 9 Difference in temperature between an anchor in a finite compaction zone and an anchor in an infinite compaction zone. The values for the compaction zone radii are R_1, R_2, R_3 and R_4 are 12, 13, 15 and 20 mm respectively. The temperature difference is expressed as a percentage of the temperature difference between the initial anchor temperature and the initial temperature of the comet water ice.

Figure 10 Comparison between anchors cooling in comet ice (no compaction zones) with flaps stowed and flaps open.

Figure 3

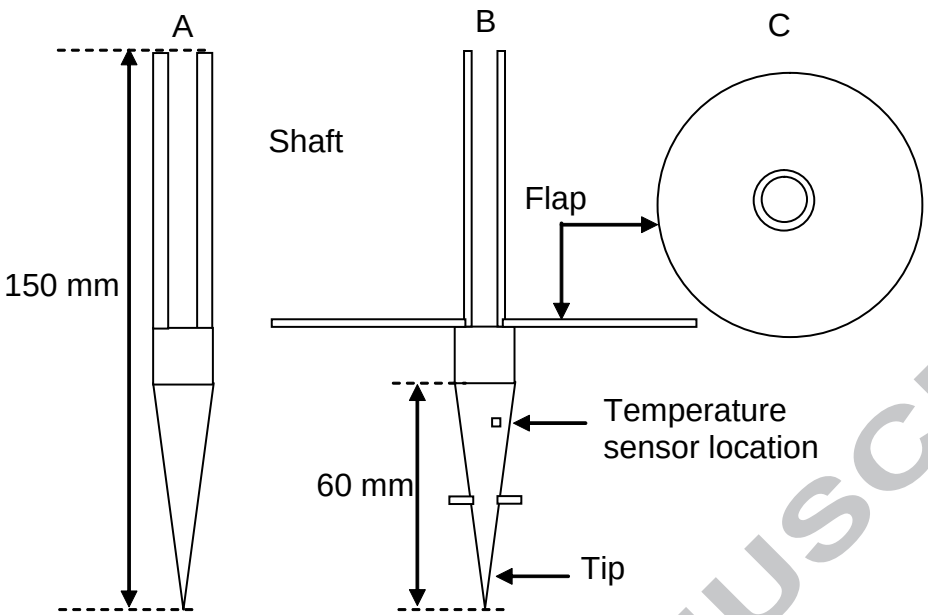

Figure 4

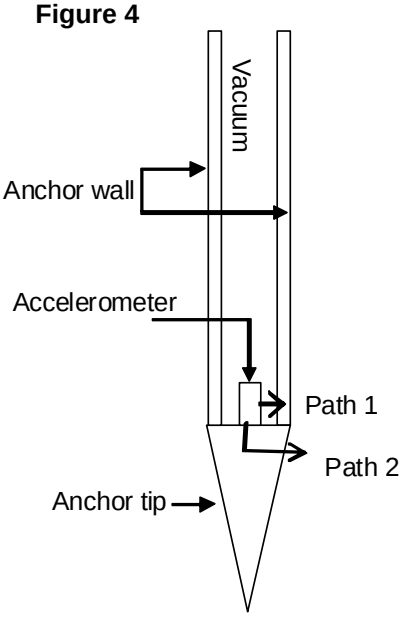

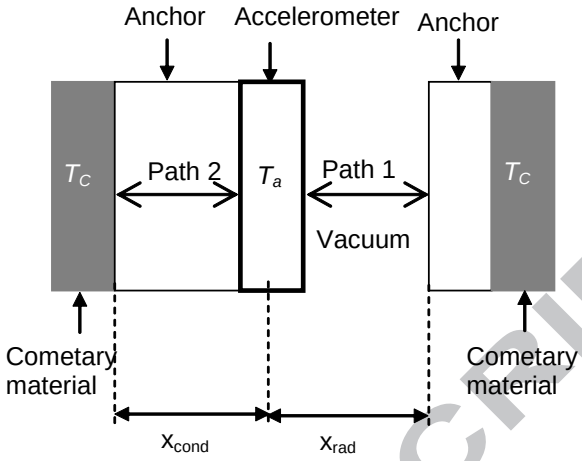

Figure 5

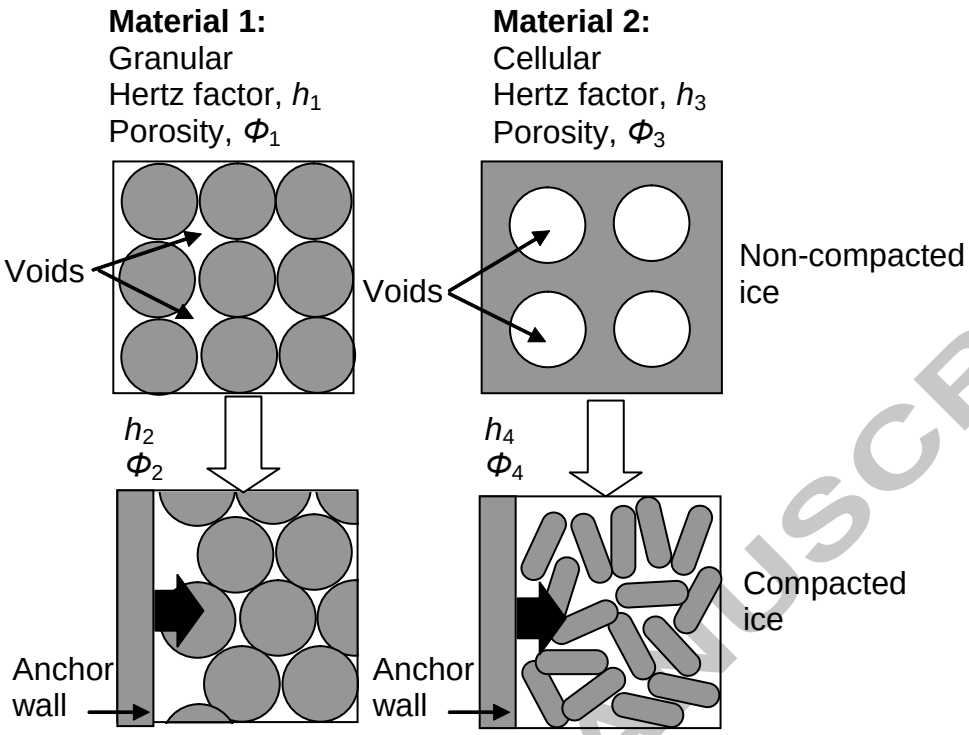

Figure 6

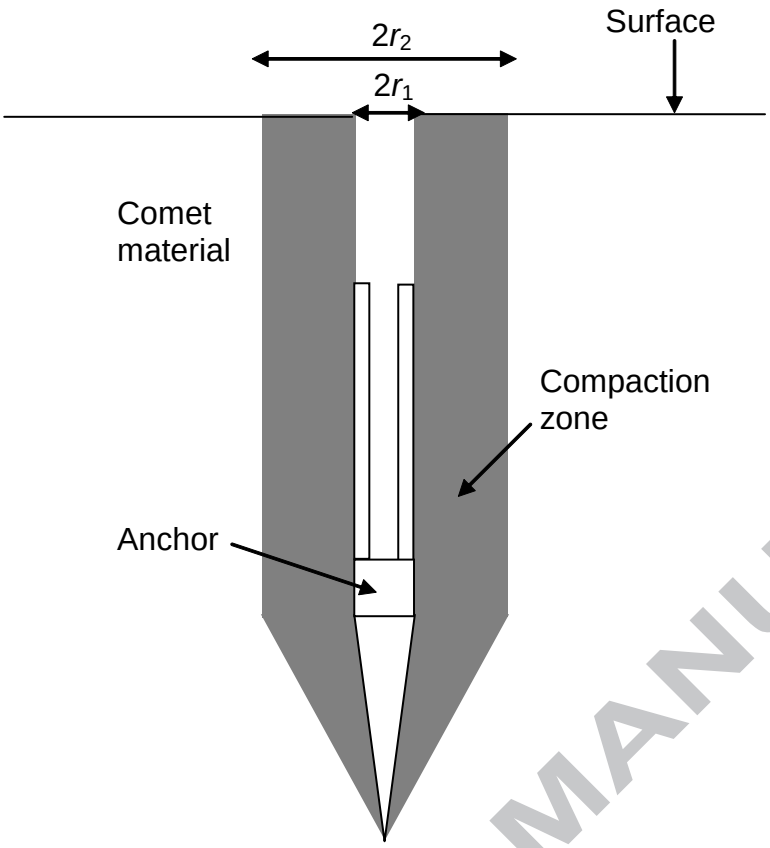

Figure 7

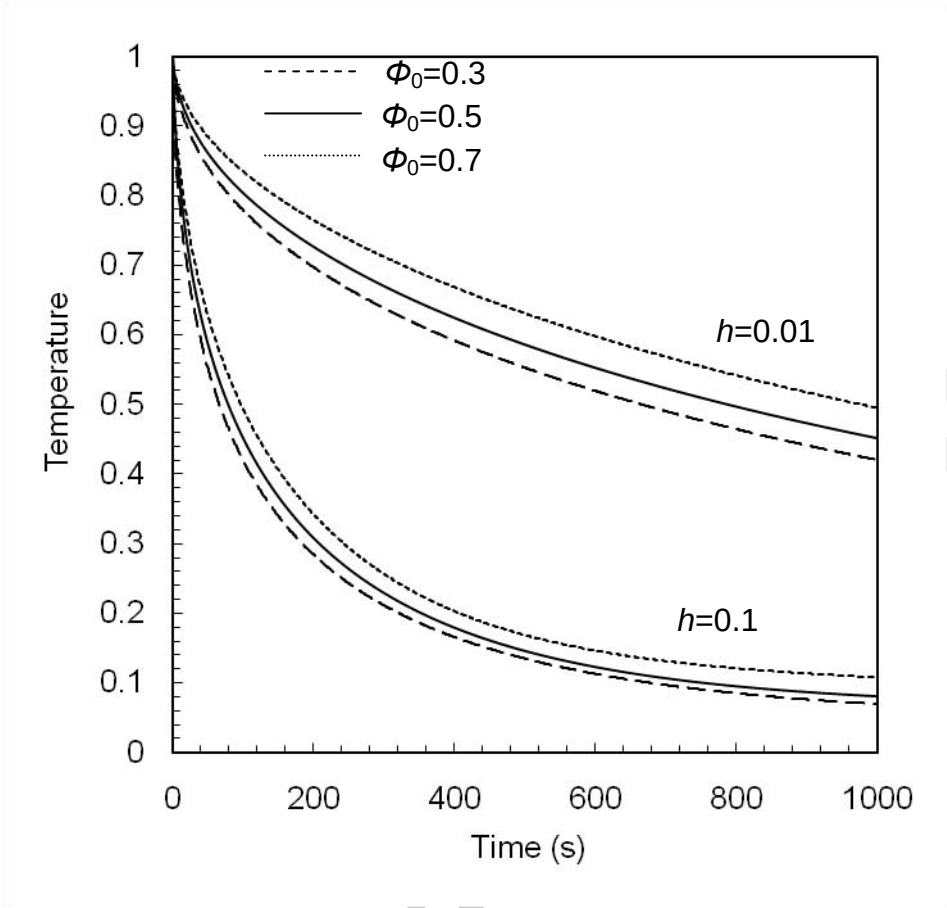

Figure 8

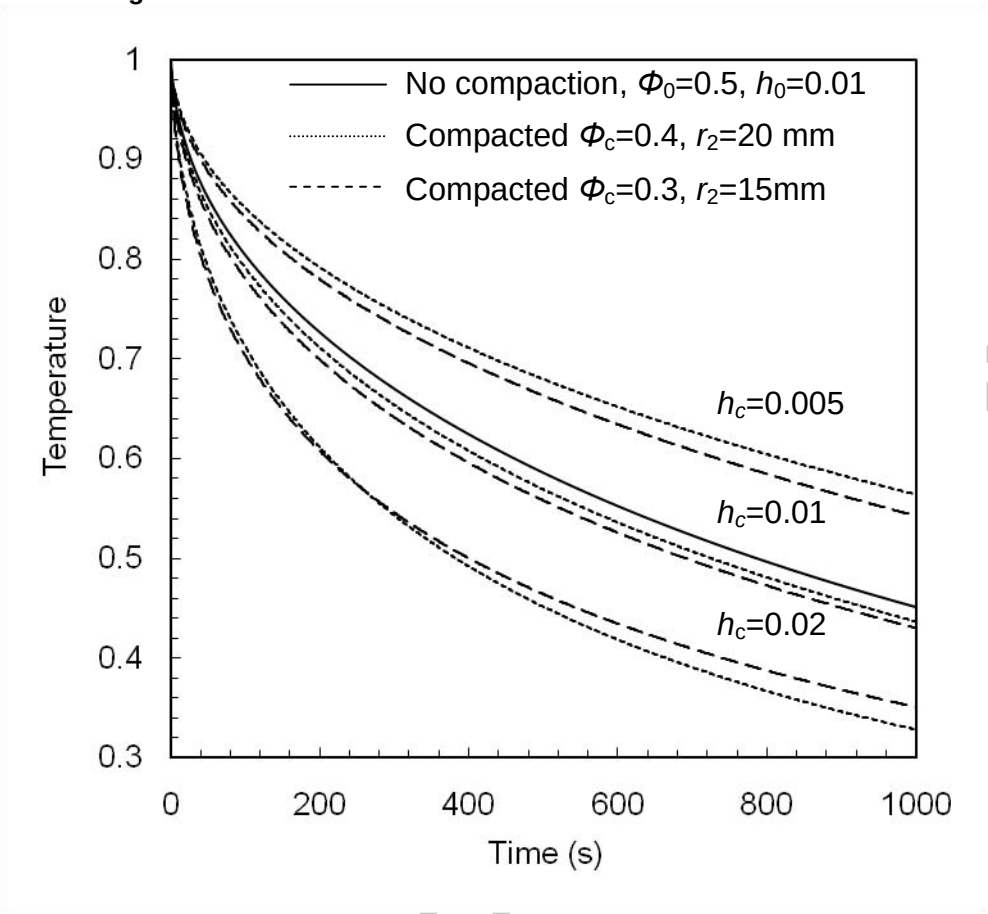

Figure 9

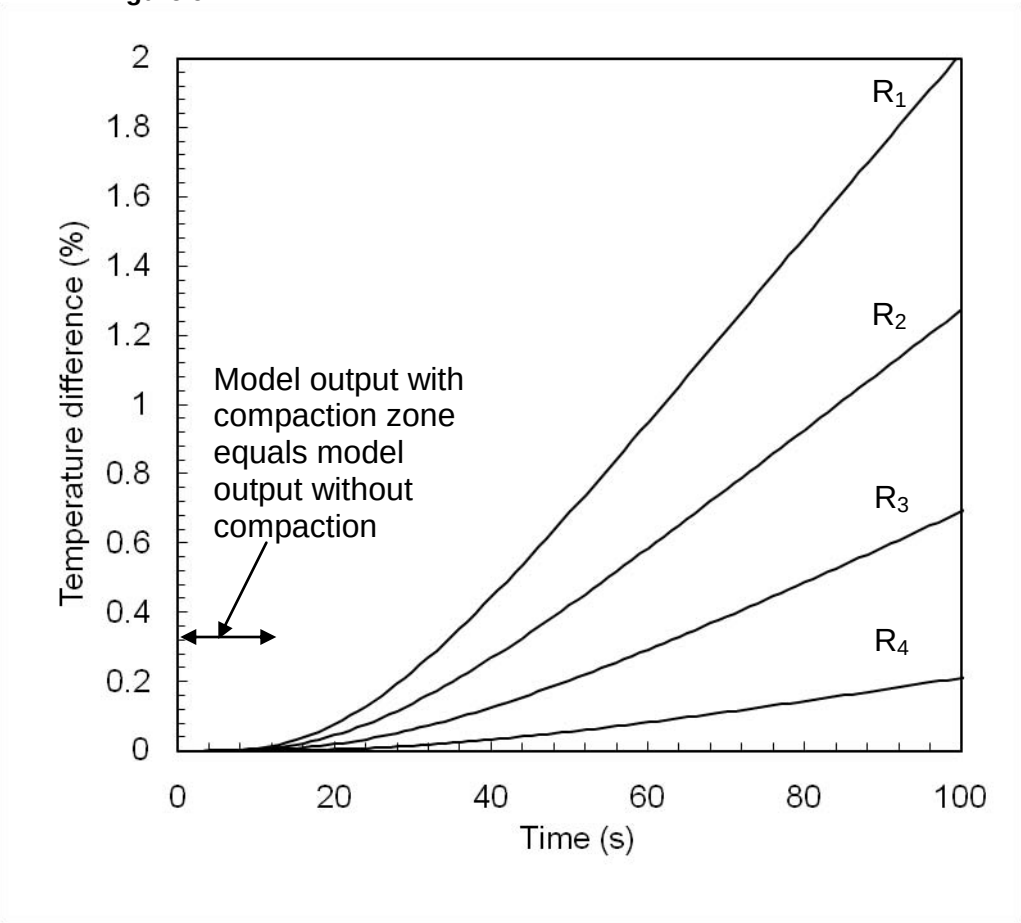

Figure 10